Acta Crystallographica Section D
Biological Crystallography
ISSN 0907-4449

Low-resolution structure determination of Na^+-translocating NADH:ubiquinone oxidoreductase from *Vibrio cholerae* by *ab initio* phasing and electron microscopy

Vladimir Y. Lunin,[a,b] Natalia L. Lunina,[a,b] Marco S. Casutt,[c] Kèvin Knoops,[d,e] Christiane Schaffitzel,[d,e] Julia Steuber,[f] Günter Fritz[c]* and Manfred W. Baumstark[a]*

[a]Department of Rehabilitative and Preventative Sports Medicine, University of Freiburg, Hugstetter Strasse 55, 79106 Freiburg, Germany, [b]Institute of Mathematical Problems of Biology, Russian Academy of Sciences, Pushchino, Moscow Region 142290, Russian Federation, [c]Department of Neuropathology, University of Freiburg, Breisacher Strasse 64, 79106 Freiburg, Germany, [d]European Molecular Biology Laboratory (EMBL), Grenoble Outstation, 6 Rue Jules Horowitz, BP 181, 38042 Grenoble CEDEX 9, France, [e]Unit of Virus Host-Cell Interactions, Unité Mixte Internationale 3265, Grenoble, France, and [f]Department of Microbiology, University of Hohenheim (Stuttgart), Garbenstrasse 30, 70599 Stuttgart, Germany

Correspondence e-mail: guenter.fritz@uniklinik-freiburg.de, maba@uni-freiburg.de

Received 5 December 2011
Accepted 20 March 2012

A low-resolution structure of the Na^+-translocating NADH:ubiquinone oxidoreductase from the human pathogen *Vibrio cholerae* was determined by *ab initio* phasing and independently confirmed by electron microscopy. This multi-subunit membrane-protein complex (molecular weight 210 kDa) generates an Na^+ gradient that is essential for substrate uptake, motility, pathogenicity and efflux of antibiotics. The obtained 16 Å resolution electron density-map revealed an asymmetric particle with a central region of low electron density and a putative detergent region, and allowed the identification of the transmembrane regions of the complex.

1. Introduction

The structure determination of large protein complexes often requires special strategies and methods (Ban *et al.*, 1998; Lunin *et al.*, 2001; Mueller *et al.*, 2007; Pedersen *et al.*, 2010) and is particularly challenging at low resolution. Weak diffraction properties of crystals are often a serious obstacle to obtaining structural information using standard methods. To overcome these difficulties, we applied an *ab initio* phasing technique (Lunin *et al.*, 1990, 2000, 2002) to study Na^+-translocating NADH:quinone oxidoreductase (Na^+-NQR).

Na^+-NQR is a central enzyme in the energy metabolism of *Vibrio cholerae*. It couples the exergonic oxidation of NADH to the transport of sodium ions (Na^+) across the membrane, generating an Na^+-motive force that is essential during infection of the human mucosa. Na^+-NQR is a membrane-protein complex consisting of six subunits (NqrA, NqrB, NqrC, NqrD, NqrE and NqrF) with a total molecular mass of about 210 kDa. It contains a [2Fe–2S] cluster and a noncovalently bound FAD, a noncovalently bound riboflavin, two covalently bound FMNs and quinone as cofactors (Bogachev *et al.*, 2001; Casutt, Huber *et al.*, 2010; Juárez *et al.*, 2008, 2009; Tao *et al.*, 2008; Türk *et al.*, 2004). To date, high-resolution structural information on Na^+-NQR is only available for part of the NqrF subunits from *Vibrio cholerae* (Tao *et al.*, 2006) and *Porphyromonas gingivalis* (PDB entry 2r6h; Midwest Center for Structural Genomics, unpublished work) and for part of the NqrC subunit from *Parabacteroides distasonis* (PDB entry 3lwx; Joint Center for Structural Genomics, unpublished work). All of the other subunits share no apparent homology with proteins of known structure. Topology studies using PhoA or GFP fusions (Duffy & Barquera, 2006), biochemical analysis and modelling studies (Casutt, Huber *et al.*, 2010; Türk *et al.*, 2004) revealed that subunits NqrB, NqrD and NqrE are

Table 1
Merging statistics for the data set used in this analysis.

To achieve 100% completeness, a few missing reflections were added from a second data set, as described in §2.

Resolution limit (Å)	Observed reflections	Unique reflections	Added reflections	$I/\sigma(I)$	R_{meas}† (%)	$R_{mrgd\text{-}F}$ (%)
37.9	173	27	2	31.87	5.10	1.90
26.8	440	51	1	35.74	6.60	2.80
21.9	586	62	1	36.59	5.60	2.10
19.0	781	72	1	32.99	6.90	2.80
17.0	920	87	1	31.98	7.40	2.00
15.5	966	88	1	30.17	8.20	2.20
14.3	1137	102	1	28.95	9.30	2.50
13.4	1174	102	1	25.85	10.70	3.10
12.6	1330	120	1	24.52	10.90	3.80
12.0	1267	114	3	23.80	11.20	3.80
8.0	15748	1889		17.25	15.70	5.60
Total	24522	2714	13	20.87	9.60	4.20

† R_{meas} and $R_{mrgd\text{-}F}$ are defined according to Diederichs & Karplus (1997).

polytopic membrane proteins, while subunits NqrC and NqrF are mainly exposed to the cytoplasm but are anchored in the membrane by a single transmembrane helix. In contrast, NqrA is associated with the membrane *via* the other subunits (Casutt, Huber *et al.*, 2010). It has been proposed that electrons from NADH are transferred to ubiquinone *via* FAD and a [2Fe–2S] cluster in NqrF, *via* FMN in NqrC and *via* FMN and riboflavin in NqrB (Juárez *et al.*, 2009).

In order to obtain structural information that will allow insights into the mechanism of this redox-driven ion pump, we crystallized the entire NQR complex (Casutt, Wendelspiess *et al.*, 2010). The crystals of Na^+-NQR had low diffractive power and only a few crystals diffracted to 4 Å resolution, a phenomenon that has been observed for many other membrane-protein crystals. After unsuccessful attempts to apply commonly used phasing methods, a more unusual *ab initio* phasing procedure was selected as a tool to obtain initial structural information. In a complementary approach, we confirmed the features observed in the X-ray structure by negative-stain electron microscopy (EM), multivariate statistical analysis (MSA; van Heel & Frank, 1981) and two-dimensional class averaging. Moreover, a three-dimensional EM reconstruction was successful using the *ab initio* electron-density map as a starting model in the reconstruction process.

2. Materials and methods

2.1. Protein preparation

Highly homogenous preparations of Na^+-NQR suitable for crystallization and EM analysis were obtained by homologous expression in *V. cholerae* and a two-step purification protocol (Tao *et al.*, 2008). His_6-tagged Na^+-NQR was crystallized by the sitting-drop vapour-diffusion technique. 2 µl protein solution at 7 mg ml^{-1} was mixed with 2 µl crystallization solution (40 m*M* KSCN, 21.0% PEG 2000 MME, 100 m*M* Tris–acetate pH 8.5, 9% 1-propanol, 10 m*M* riboflavin, 1% *N*,*N*-dimethylformamide) at 277 K. Crystals appeared after 5–7 d and grew to their final size of 30 × 80 × 200 µm after 15 d. Na^+-NQR crystals were flash-cooled in liquid nitrogen after soaking in crystallization solution supplemented with 30% PEG 550 MME. Crystals of Na^+-NQR diffracted to 4.0 Å resolution and belonged to space group $P2_1$, with unit-cell parameters a = 94, b = 146, c = 105 Å, $\alpha = \gamma = 90$, $\beta = 111^\circ$ (Casutt, Wendelspiess *et al.*, 2010).

2.2. Data collection

Data sets were collected from Na^+-NQR crystals on beamline ID14-4 at the ESRF, Grenoble, France using a previously described setup (Ritter *et al.*, 1999). Briefly, the combination of a helium tube and a small beam stop placed at the detector side of the helium tube allows data collection between 300 and 8 Å resolution on beamline ID14-4, which provides a clean beam of low divergence. In order to avoid overloads of strong reflections but to obtain reliable intensities for weak reflections, three passes recorded at different X-ray fluxes were merged. Highly redundant data sets were collected from several Na^+-NQR crystals and two of them were used in this analysis. The data set with the best statistics with regard to $I/\sigma(I)$ and R factors was selected for *ab initio* phase analysis. However, owing to the orientation of the crystal in the beam, a few reflections were missing. After scaling the data sets (correlation of 0.935), a few reflections (Table 1) from a data set of lower quality were added to the first data set in order to estimate the intensity of the missing reflections but to preserve the good R_{meas} of the first data set. The reflections estimated from the second crystal are marked by flag value 1 in the data set deposited as Supplementary Material[1]. All data were integrated and scaled with *XDS* (Kabsch, 2010*a*,*b*). Data statistics are given in Table 1.

2.3. Phasing

To obtain initial X-ray structural information on Na^+-NQR, an *ab initio* low-resolution phasing procedure (Lunin *et al.*, 1990, 2002) was applied. This approach allows the determination of a few hundred low-resolution phases based on experimental structure-factor magnitudes and certain general properties of macromolecular crystal structures. The reported phasing procedure is based on the observation that a high-density region in a phased Fourier synthesis is composed of a small number of connected components (Baker *et al.*, 1993; Lunin *et al.*, 2000). The whole phasing procedure starts from a few dozen lowest resolution reflections and proceeds through several steps, gradually increasing the number of reflections involved and tightening the selection criteria. At every step a large number of phase sets (*e.g.* several million) are randomly generated. For each generated set the corresponding Fourier synthesis and the number of connected components in the high-density region are calculated as well as the component dimensions. A phased set is considered as 'admissible' and stored for further analysis if the corresponding Fourier synthesis has satisfactory connectivity properties. The process

[1] Supplementary material has been deposited in the IUCr electronic archive (Reference: WD5173). Services for accessing this material are described at the back of the journal.

of phase-set generation is continued until the desired number of admissible phase sets (100 in the reported work) has been obtained.

After the selected admissible phase sets had been aligned by permitted space-group origin shifts (Lunin & Lunina, 1996) the 'best' (centroid) phase value $\varphi^{\rm best}(\mathbf{h})$ and 'figure of merit' $m(\mathbf{h})$ (Blow & Crick, 1959; Lunin *et al.*, 1990) were calculated for every reflection. The figure of merit is equal to the mean cosine value of the deviation of phase $\varphi(\mathbf{h})$ from $\varphi^{\rm best}(\mathbf{h})$ over the selected sets. It reflects the uncertainty in the determination of $\varphi^{\rm best}(\mathbf{h})$: the higher the $m(\mathbf{h})$ value, the more unambiguously the phase has been determined. It may be used to monitor phase improvement from step to step and as a weighting factor when calculating Fourier syntheses.

In the phase-set generation process, every phase value is generated with its individual probability distribution, which is updated after every phasing step (Lunin *et al.*, 2002). Generally, the reflections were generated according to the Von Mises distribution (Evans *et al.*, 2000), with the parameter value adapted so that the expected value of the cosine of the phase deviation from $\varphi^{\rm best}(\mathbf{h})$ is equal to that found at the end of the previous step. The exception is the case where a new reflection is included in phasing for the first time. In this case the probability distribution is supposed to be uniform.

Our estimate of the achieved resolution is based on the observation (Lunin & Woolfson, 1993) that newly phased reflections (*e.g.* from a new resolution shell) improve the quality of the Fourier synthesis if their map correlation coefficient is greater than half the correlation coefficient for previously phased reflections: $C_{\rm new} \geq 0.5C_{\rm old}$. Strictly speaking this condition is just a sufficient condition, but in practice it is close to a necessary and sufficient condition to improve the resulting map. A simple consequence of this rule is that the correlation $C_{\rm new} \geq 0.5$ is enough to obtain an improved map after new resolution-shell reflections have been added to the synthesis.

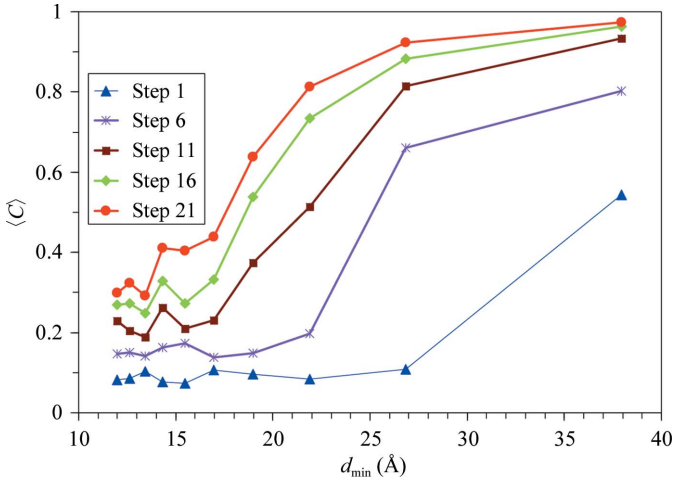

Figure 1
Statistics during the course of phasing. The expected value of the shell correlation coefficient $\langle C\rangle = \sum_{\mathbf{h}\ \text{in the shell}}[F_{\rm obs}(\mathbf{h})]^2 m(\mathbf{h}) / \sum_{\mathbf{h}\ \text{in the shell}}[F_{\rm obs}(\mathbf{h})]^2$ *versus* the resolution shells is shown after one, six, 11, 16 and 21 cycles of phase calculation.

The phasing procedure for Na^+-NQR consisted of 21 cycles. In the first cycle just 32 reflections in the 36 Å resolution zone were used; the number of reflections was increased step by step to 1267 reflections in the 12 Å resolution zone. In the initial cycles, the high-density region was defined as the 15% of grid points possessing the highest values in the Fourier synthesis. It was extended to 20% of points in the last cycles. The selection rule applied allows a high-density region composed of only two connected components of equal volume. Similar to some other phasing methods, the problem regarding the choice of the correct enantiomer also arises in *ab initio* phasing. It should be noted that the obtained resolution of the Fourier syntheses at present does not allow an unambiguous choice between the two possible enantiomers. The experimentally obtained structure-factor magnitudes and *ab initio* determined phases corresponding to different steps of the phasing procedure are provided as Supplementary Material (data set 1).

2.4. Negative-stain EM and image processing

Na^+-NQR was centrifuged for 18 h at 34 000 rev min^{-1} (SW60 Ti Rotor, Beckman Coulter, 148 300*g*) into a 10–30% glycerol and 0–0.15% glutaraldehyde gradient (Kastner *et al.*,

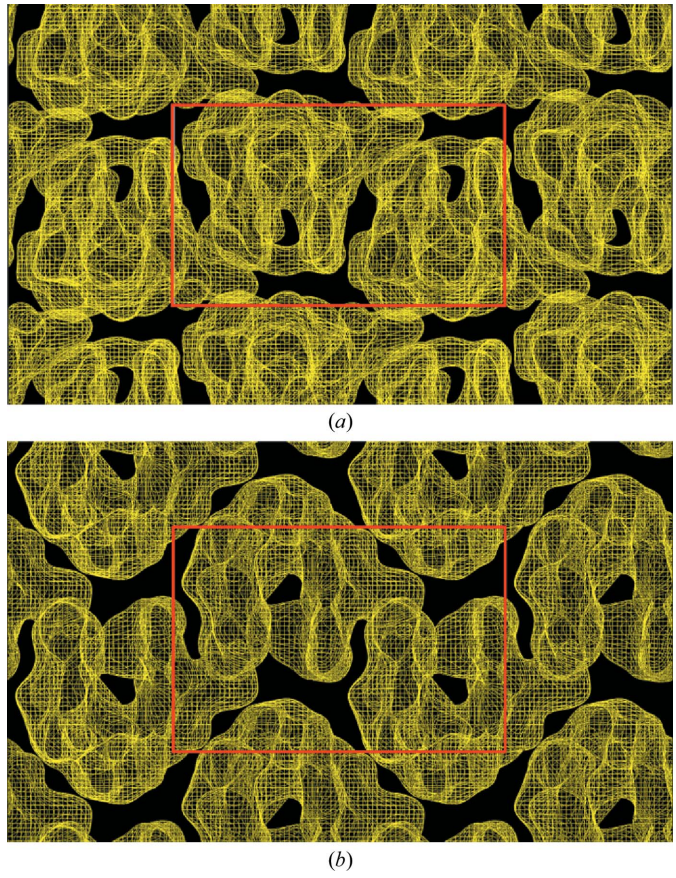

Figure 2
Na^+-NQR electron-density map at a resolution of 16 Å calculated by *ab initio* phasing. Projections of *ab initio*-phased electron-density synthesis along the crystallographic axes **c** (*a*) and **a** (*b*) are shown. The unit cell is indicated by a red box.

2008) for limited cross-linking. After centrifugation, the reaction was stopped by the addition of 100 µg ml^{-1} lysine (Sigma). The peak fractions were analysed by negative-stain EM. The complexes were absorbed onto carbon film for 30 s followed by negative staining with 1% uranyl acetate for 30 s. 160 micrographs of the complex were recorded under low-dose conditions with a bottom-mounted Orios SC600 camera (Gatan Inc.) in a Jeol 1200EX II transmission electron microscope running at 100 kV at a magnification of 40 000× (pixel size of 1.7 Å). A total of 10 302 individual Na^+-NQR complexes were selected with *Boxer* (*EMAN* suite; Ludtke *et al.*, 1999) from the micrographs, low-pass filtered to 13 Å and processed with *IMAGIC*-5 (Image Science; van Heel *et al.*, 1996). After an initial 'reference-free' alignment procedure, the particles were iteratively subjected to multivariate statistical analysis and classification. Selected two-dimensional class averages were used as reference images for the subsequent rounds of alignment, resulting in 120 two-dimensional class averages (van Heel & Frank, 1981). The two-dimensional class averages were compared with different views of the *ab initio* electron-density map. An initial three-dimensional reconstruction of the Na^+-NQR complex was calculated using the X-ray structural information of Na^+-NQR, which was low-pass filtered to 35 Å, as a starting reference structure. This initial EM reconstruction was further refined using the program *SPIDER* (Frank *et al.*, 1996). The resulting angular distribution map of the images showed a strong preference for certain views, which was corrected by restricting the number of particle projections in each direction. The final reconstruction is based on 9772 particles.

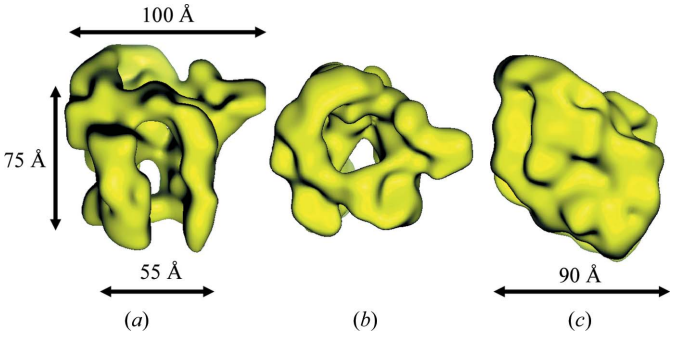

Figure 3
A 16 Å resolution envelope for one Na^+-NQR particle: (*a*) side view, (*b*) top view, (*c*) side view rotated 90°.

2.5. Molecular graphics

Figures were prepared using *UCSF Chimera* (Pettersen *et al.*, 2004) and *PyMOL* (DeLano, 2002).

3. Results

An *ab initio* phasing procedure applied to the complete set of low-resolution reflections collected between 12 and 97 Å yielded initial information on the three-dimensional structure of the Na^+-NQR complex. The effective resolution of the resulting map was defined as 16 Å based on analysis of the resolution-shell correlation coefficient (Lunin & Woolfson, 1993; Fig. 1). The resulting electron-density map revealed the shape of the Na^+-NQR complex and the packing of particles in the unit cell (Fig. 2). The observed particle is highly asymmetric and reveals a region of low electron density in the centre (Fig. 3). The particle has a height of 75 Å; the width is ∼55 Å in the lower region and ∼100 Å in the upper part with the pronounced protrusion. The depth of the particle is approximately 90 Å. Overall, the dimensions of the particle fit well to a protein complex with a molecular mass of 210 kDa (Lazarov *et al.*, 2006).

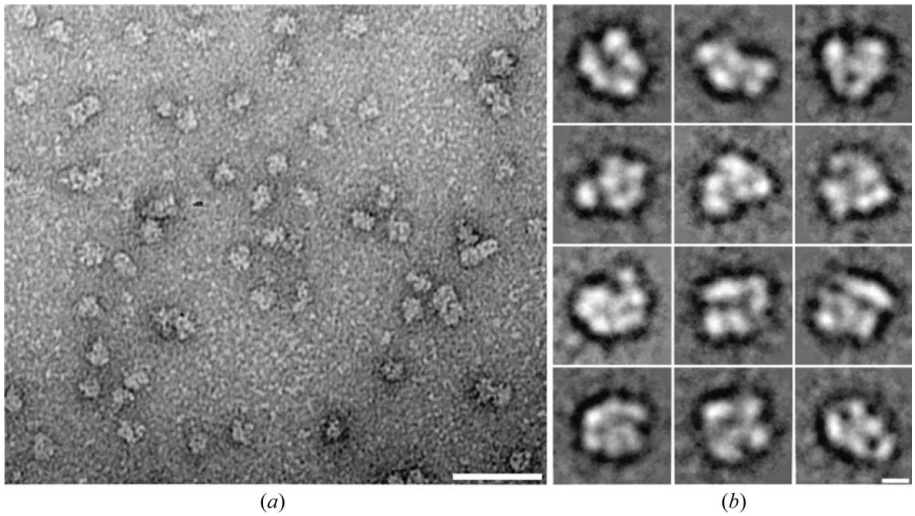

Figure 4
Electron microscopy of the Na^+-NQR complex stained with 1% uranyl acetate. (*a*) Micrographs of GraFix-pretreated Na^+-NQR complexes show uniform particles with a diameter of 100–150 Å. (*b*) Characteristic two-dimensional class averages of the complex reveal asymmetric particles consisting of multiple domains. The scale bars are 500 Å in the overview and 50 Å for the two-dimensional class averages.

3.1. Electron microscopy of the Na^+-NQR complex

To confirm our findings, we analysed the Na^+-NQR complex by EM. In negative-stain EM, homogenous particles with a diameter of about 100–150 Å were identified (Fig. 4). MSA and two-dimensional class averaging yielded particles (Fig. 4) with features particularly similar to certain views of the *ab initio*-calculated molecular envelope (Fig. 5), namely an asymmetric particle with a central cavity (Fig. 2). The overall similarity of the EM and X-ray data was further confirmed by the calculation of a three-dimensional reconstruction, in which the X-ray structure (filtered to 35 Å) was used as an initial reference model (Fig. 6). The final reconstruction

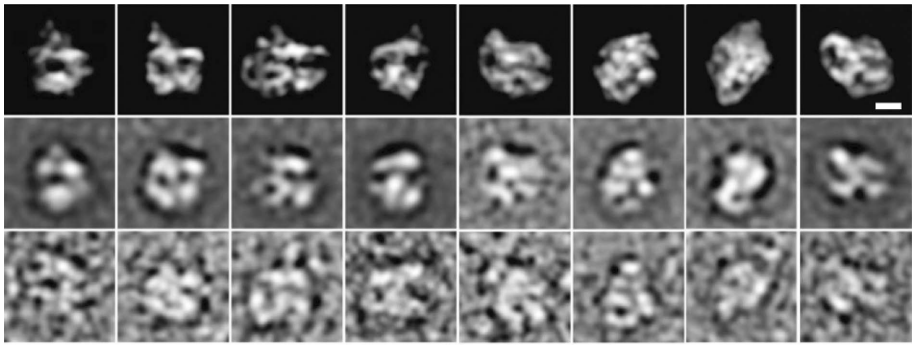

Figure 5
Comparison of EM two-dimensional class averages and equivalent views of the Na^+-NQR complex in the X-ray structure. The projection of the Na^+-NQR crystal structure (top) is depicted next to the most similar EM two-dimensional class average (middle) and an individual Na^+-NQR particle that has been filtered to 13 Å and aligned with the two-dimensional class average (bottom). Two-dimensional class averages with a particularly pronounced resemblance to certain views of the X-ray map are depicted. The scale bar represents 50 Å.

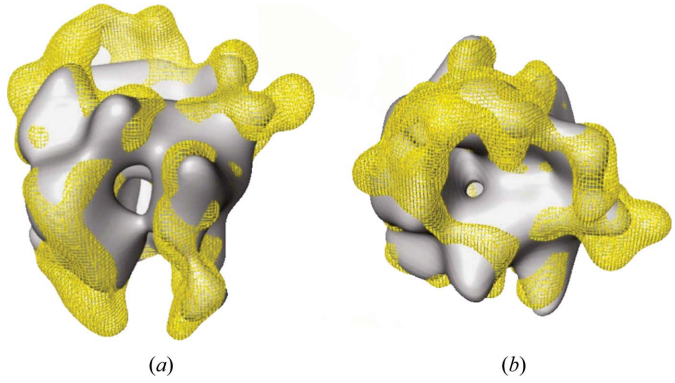

Figure 6
Overlay of the 16 Å crystal structure (yellow) and the EM reconstruction (grey) showing similar features and dimensions of the Na^+-NQR complex. The 35 Å filtered X-ray map was used as an initial model for alignment of the Na^+-NQR particles. (*a*) Side view, (*b*) top view of the Na^+-NQR complex.

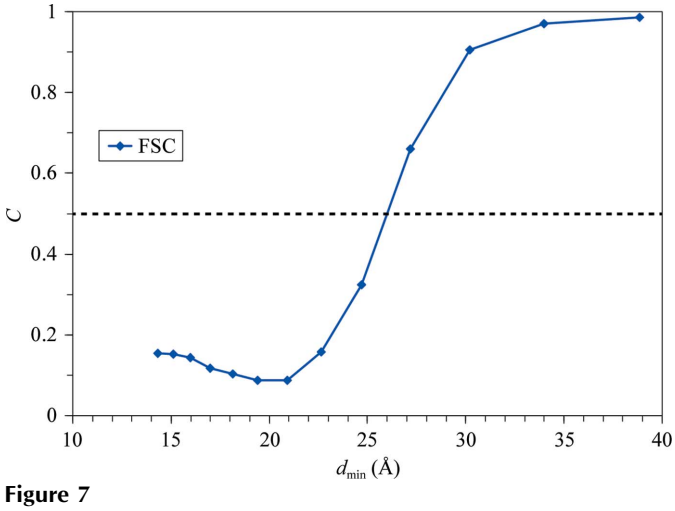

Figure 7
Diagram of the Fourier shell correlation (FSC) function computed between two independent three-dimensional reconstructions of the Na^+-NQR complex (blue line). The set of 9772 particles was randomly split into two half sets to calculate the two reconstructions. FSC = 0.5 (dotted line) indicates 26 Å resolution.

is based on 9772 particles and has a resolution of 26 Å as estimated by the Fourier shell correlation (FSC) = 0.5 criterion (Fig. 7). The EM reconstruction displays similar dimensions and features to the Na^+-NQR complex structure obtained by *ab initio* phase determination.

3.2. Low-resolution imaging of detergent regions in the crystal

Membrane-protein crystals contain a large proportion of detergent and often some lipids. The detergent is frequently present in layers but is not visible in high-resolution structures owing to disorder on the atomic scale. Nevertheless, there is some degree of order at the molecular level that makes these regions likely to be observed at lower resolution. Aqueous buffer has an electron density of about 340 e nm^{-3}, whereas acyl chains have a lower electron density of about 280 e nm^{-3} (Luzzati *et al.*, 1979). The detergent layer therefore has negative contrast with respect to the solvent. Fig. 8 presents the distribution of the lowest value regions in the 16 Å resolution electron-density map. These regions form clearly separated parallel layers of about 54 Å in thickness, which fit well to the proportions of a dodecyl maltoside bilayer. Such detergent bilayers were observed in membrane-protein crystals (Caffrey, 2000) in which the protein/detergent micelles fuse and form a laminar liquid crystalline phase. As expected for a detergent layer, the protein molecules are embedded in these planes. The position of the proteins in the planes provides information about the localization of the transmembrane regions. For the Na^+-NQR complex the hydrophobic part was mapped to the lower narrow part (Fig. 8), whereas the larger upper part is exposed to the solvent. This arrangement is likely to resemble the *in vivo* situation in the cytoplasmic membrane, with the exception that in the crystal the neighbouring particles are present in alternating orientations linked by the crystallographic dyad (Fig. 2).

4. Discussion

Usually, the phase information in protein X-ray crystallography is obtained from molecular replacement or heavy-atom derivatives. These methods are often combined for protein complexes at low resolution, or phase information from other sources is included for structure determination. For instance, in the case of the large ribosomal subunit, phases from an EM structure were used to map the heavy-atom positions of the derivatives (Ban *et al.*, 1998). In the case of Na^+-NQR, where only a small part of the entire complex is structurally well characterized, molecular replacement fails to provide sufficient phase information. Therefore, heavy-atom derivatization of the crystals is required. However, the search

for heavy-atom derivatives is often a time-consuming and tedious undertaking. In particular, membrane-protein crystals are very fragile and sensitive to manual manipulation. Moreover, the insertion of heavy atoms may destroy the lattice and lead to very low residual diffraction. In this study, we show that it is possible to obtain phases and thus calculate a low-resolution structure from the original non-derivatized crystals using *ab initio* phase determination.

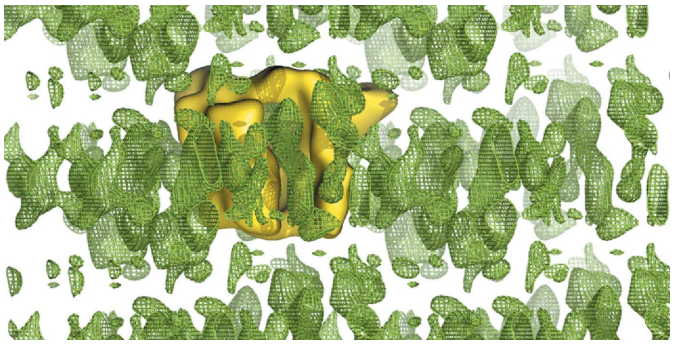

Figure 8
Localization of detergent layers in the crystal. The distribution of the low-density regions in the crystal is shown in green. This density corresponds to detergent regions with lower electron density than the aqueous solvent forming distinct parallel layers. Electron density for one protein particle is depicted as a yellow surface, showing that protein particles and detergent layers colocalize in the crystal.

The phasing procedure applied in this study has been developed over recent decades and various aspects of the procedure have been the subject of previous publications (a recent review of the approach may be found in Lunin *et al.*, 2012). The method has been tested on known structures, including large macromolecular complexes such as the ribosomal T50S particle (Lunin *et al.*, 2002), the $tRNA^{Asp}$–aspartyl-tRNA synthetase complex (Fokine *et al.*, 2003) and the transporter AcrB (Lunin *et al.*, 2007). Unfortunately, in its current state the procedure is laborious and requires the completeness of very low-resolution data, which are often neglected using standard data-collection setups. These conditions place it outside the routine tools of structure analysis, but leave room for cases where standard methods fail.

Selection criteria based on properties of electron-density distributions (histograms, connectivity *etc.*) may be rather sensitive to the absence of even a small number of very strong reflections. Such very strong reflections usually fill the lowest resolution range of reciprocal space and a special effort should be made to measure them correctly, or at least to estimate their values. In the case of Na^+-NQR described here, the absence of a few reflections from the data set does not seem to be crucial for the success of phasing. Fig. 9(*a*) illustrates the effect of missing reflections: the envelopes obtained from the data set without any reflections added and complemented with reflections from the second data set are shown. Some differences between the two envelopes are observed, but the general features of the solution are unchanged.

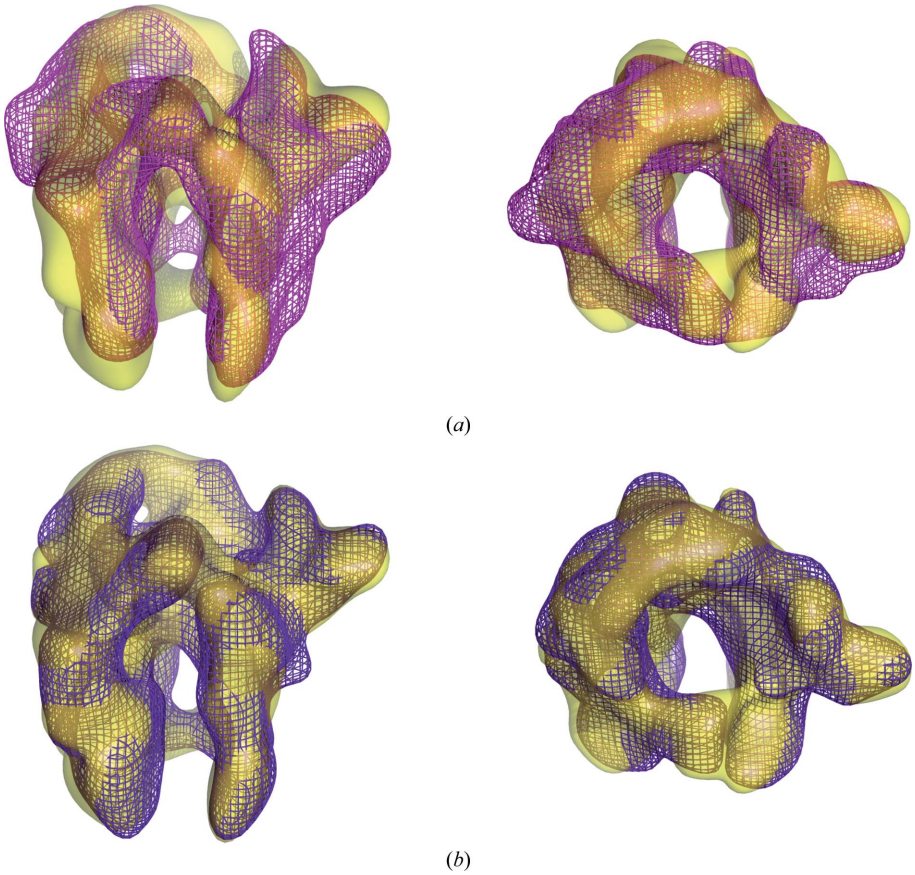

Figure 9
Comparison of 16 Å resolution envelopes for Na^+-NQR obtained with different protocols after 15 cycles of phasing. (*a*) Overlay of envelopes calculated from a single data set with missing reflections in the low-resolution sphere (magenta) or from the same data after the addition of 13 reflections estimated from a different crystal (yellow). The observed differences illustrate the importance of the completeness of low-resolution reflections. (*b*) Overlay of envelopes obtained applying slightly different phasing parameters. Both envelopes are essentially the same, underlining the robustness of the method.

The merging of data sets collected from different crystals may be a risky business even when working with crystals of reproducible quality (Giordano *et al.*, 2012). In the case of membrane-protein crystals one has to be cautious since differing solvent/detergent contents can lead to slightly different packing in the crystals and merging of data would largely blur the signal. In view of such potential complications, we avoided merging data from different crystals. A few reflections collected from a second crystal served as estimates of the corresponding values in the first data set. Systematic analysis of the

added reflections revealed that only three of the 13 added reflections might have been crucial for connectivity-based phasing.

The phasing protocol includes some tuneable parameters (random-number generator seed, a cutoff used to obtain a molecule mask in the generated Fourier synthesis, increments in resolution from step to step *etc.*). Our previous tests revealed that the approach is sufficiently robust and stable with respect to small changes in the different parameters. The results of *ab initio* phasing applying two slightly different parameter sets are shown in Fig. 9(*b*). Basically, there is no difference between the two solutions.

A further potential pitfall in the applied phasing procedure is the extension of resolution from low (20–16 Å) to medium (12–10 Å) resolution. Increasing the resolution of Fourier maps does not necessarily facilitate interpretation of the electron-density maps, especially if the obtained resolution is still too low to identify secondary-structure elements. In such cases a 16 Å envelope is more instrumental since the features of the molecular envelope are preserved. Some successful attempts to extend low-resolution phases to medium resolution have been made, but it must be noted that these were small proteins (Lunin *et al.*, 2002). In *ab initio* phasing of large complexes it is still a major challenge to overcome the barrier close to 16 Å resolution.

In addition to the information traditionally obtained from diffraction data, membrane-protein crystals may also provide structural information on the localization of the detergent with respect to the protein molecules. Detergent in membrane-protein crystals has been visualized previously using neutron diffraction (Roth *et al.*, 1989; Timmins, 1995). However, neutron diffraction requires rather large crystals, which are often not available, in particular in the case of membrane proteins. As we show here, low-resolution *ab initio* phasing can map the distribution of the detergent in the crystal and thereby helps to localize the transmembrane parts of proteins or complexes.

Topology studies revealed that Na^+-NQR is asymmetric with respect to the distribution of the hydrophilic domains. The major portion of the hydrophilic domains reside at the cytosolic side, while the periplasmic side of Na^+-NQR is essentially characterized by short loops (Casutt, Huber *et al.*, 2010; Türk *et al.*, 2004; Duffy & Barquera, 2006). The position of the protein particle in the observed detergent layer agrees well with the topology studies and allows putative mapping of the subunits in the particle. According to these data, the electron density at the top of the particle, with its noticeable protrusions (Figs. 3 and 8), corresponds to the hydrophilic domains, whereas the loops at the periplasmic aspect of Na^+-NQR correspond to the bottom of the particle. Information on the location of the subunits in the particle and on the packing of the particle in the crystal represents a basis for rational improvement of crystal quality. Regions in the protein particle devoid of hydrophilic domains can be engineered by fusion of hydrophilic proteins, yielding improved crystal packing and accordingly better diffraction properties (Rosenbaum *et al.*, 2007; Derewenda, 2010).

Three-dimensional structures obtained by EM methods are often considered as prospective preliminary models for subsequent crystallographic studies. In our case, we reversed this order and used negative-stain EM information for the validation of results obtained by X-ray methods. Independently calculated two-dimensional class averages of the Na^+-NQR complex agree very well with the crystal structure (Figs. 4 and 5). A 26 Å resolution three-dimensional reconstruction based on the X-ray map at 35 Å resolution as an initial model shows similar features and dimensions (Fig. 6), with the exception of three protruding elements which are not present in the EM structure. These protrusions are not or are poorly visible in the individual images of the Na^+-NQR complex and in the two-dimensional class averages (Fig. 5). It is likely that these regions of the Na^+-NQR complex are poorly stained by uranyl acetate, or they may exhibit intrinsic flexibility resulting in different conformations. Consequently, the density is not visible in the three-dimensional reconstruction as it is averaged out. It is noteworthy that the packing of the particles in the crystal suggests that some of these protruding elements are involved in crystal contacts and are thereby constrained to a single conformation in the crystal lattice.

In summary, *ab initio* low-resolution phasing can provide important structural information in many X-ray crystallographic projects where the molecule of interest is a membrane protein or membrane-protein complex yielding crystals of low diffractive power. The size and shape of the particle is accessible using the native data. In the case of membrane proteins the localization of detergent or lipid in the crystal may also be observed. The future aim is to refine the method to allow phase extension to higher resolution and combination with other phasing techniques.

We thank the staff at beamline ID14-4 at the ESRF for excellent support. This work was partly supported by Russian Foundation for Basic Research grant 10-04-00254-a (to VYL and NLL), by Swiss National Science Foundation grant PP0033-118994 (to JS), by European Molecular Biology Organization postdoctoral fellowship ALTF 900-2009 (to KK), by Deutsche Forschungsgemeinschaft grants BA 1866/4-1 and 5-1 (to MWB), by contract research 'Methoden in den Lebenswissenschaften' of the Baden-Württemberg Stiftung (to JS, CS and GF) and by Deutsche Forschungsgemeinschaft grant FR 1488/3-1 (to GF).

References

Baker, D., Krukowski, A. E. & Agard, D. A. (1993). *Acta Cryst.* D**49**, 186–192.
Ban, N., Freeborn, B., Nissen, P., Penczek, P., Grassucci, R. A., Sweet, R., Frank, J., Moore, P. B. & Steitz, T. A. (1998). *Cell*, **93**, 1105–1115.
Blow, D. M. & Crick, F. H. C. (1959). *Acta Cryst.* **12**, 794–802.
Bogachev, A. V., Bertsova, Y. V., Barquera, B. & Verkhovsky, M. I. (2001). *Biochemistry*, **40**, 7318–7323.
Caffrey, M. (2000). *Curr. Opin. Struct. Biol.* **10**, 486–497.
Casutt, M. S., Huber, T., Brunisholz, R., Tao, M., Fritz, G. & Steuber, J. (2010). *J. Biol. Chem.* **285**, 27088–27099.
Casutt, M. S., Wendelspiess, S., Steuber, J. & Fritz, G. (2010). *Acta Cryst.* F**66**, 1677–1679.

DeLano, W. L. (2002). *PyMOL*. http://www.pymol.org.
Derewenda, Z. S. (2010). *Acta Cryst.* D**66**, 604–615.
Diederichs, K. & Karplus, P. A. (1997). *Nature Struct. Biol.* **4**, 269–275.
Duffy, E. B. & Barquera, B. (2006). *J. Bacteriol.* **188**, 8343–8351.
Evans, M., Hastings, N. & Peacock, B. (2000). *Statistical Distributions*, 3rd ed., pp. 189–191. New York: Wiley.
Fokine, A., Lunina, N., Lunin, V. & Urzhumtsev, A. (2003). *Acta Cryst.* D**59**, 850–858.
Frank, J., Radermacher, M., Penczek, P., Zhu, J., Li, Y., Ladjadj, M. & Leith, A. (1996). *J. Struct. Biol.* **116**, 190–199.
Giordano, R., Leal, R. M. F., Bourenkov, G. P., McSweeney, S. & Popov, A. N. (2012). *Acta Cryst.* D**68**, 649–658.
Heel, M. van & Frank, J. (1981). *Ultramicroscopy*, **6**, 187–194.
Heel, M. van, Harauz, G., Orlova, E. V., Schmidt, R. & Schatz, M. (1996). *J. Struct. Biol.* **116**, 17–24.
Juárez, O., Morgan, J. E. & Barquera, B. (2009). *J. Biol. Chem.* **284**, 8963–8972.
Juárez, O., Nilges, M. J., Gillespie, P., Cotton, J. & Barquera, B. (2008). *J. Biol. Chem.* **283**, 33162–33167.
Kabsch, W. (2010*a*). *Acta Cryst.* D**66**, 125–132.
Kabsch, W. (2010*b*). *Acta Cryst.* D**66**, 133–144.
Kastner, B. *et al.* (2008). *Nature Methods*, **5**, 53–55.
Lazarov, V. K., Fraering, P. C., Ye, W., Wolfe, M. S., Selkoe, D. J. & Li, H. (2006). *Proc. Natl Acad. Sci. USA*, **103**, 6889–6894.
Ludtke, S. J., Baldwin, P. R. & Chiu, W. (1999). *J. Struct. Biol.* **128**, 82–97.
Lunin, V. Yu. & Lunina, N. L. (1996). *Acta Cryst.* A**52**, 365–368.
Lunin, V. Y., Lunina, N., Podjarny, A. D., Bockmayr, A. & Urzhumtsev, A. (2002). *Z. Kristallogr.* **217**, 668–685.
Lunin, V. Y., Lunina, N. L., Ritter, S., Frey, I., Berg, A., Diederichs, K., Podjarny, A. D., Urzhumtsev, A. & Baumstark, M. W. (2001). *Acta Cryst.* D**57**, 108–121.
Lunin, V. Y., Lunina, N. L. & Urzhumtsev, A. G. (2000). *Acta Cryst.* A**56**, 375–382.
Lunin, V. Y., Lunina, N. & Urzhumtsev, A. (2007). *Evolving Methods for Macromolecular Crystallography*, edited by R. J. Read & J. L. Sussman, pp. 123–133. Dordrecht: Springer.
Lunin, V. Y., Urzhumtsev, A. G. & Podjarny, A. (2012). *International Tables for Crystallography*, Vol. *F*, 2nd online ed., edited by E. Arnold, D. M. Himmel & M. G. Rossmann, pp. 437–442. Chester: International Union of Crystallography
Lunin, V. Yu., Urzhumtsev, A. G. & Skovoroda, T. P. (1990). *Acta Cryst.* A**46**, 540–544.
Lunin, V. Yu. & Woolfson, M. M. (1993). *Acta Cryst.* D**49**, 530–533.
Luzzati, V., Tardieu, A. & Aggerbeck, L. P. (1979). *J. Mol. Biol.* **131**, 435–473.
Mueller, M., Jenni, S. & Ban, N. (2007). *Curr. Opin. Struct. Biol.* **17**, 572–579.
Pedersen, B. P., Morth, J. P. & Nissen, P. (2010). *Acta Cryst.* D**66**, 309–313.
Pettersen, E. F., Goddard, T. D., Huang, C. C., Couch, G. S., Greenblatt, D. M., Meng, E. C. & Ferrin, T. E. (2004). *J. Comput. Chem.* **25**, 1605–1612.
Ritter, S., Diederichs, K., Frey, I., Berg, A., Keul, J. & Baumstark, M. (1999). *J. Cryst. Growth*, **196**, 344–349.
Rosenbaum, D. M., Cherezov, V., Hanson, M. A., Rasmussen, S. G. F., Thian, F. S., Kobilka, T. S., Choi, H.-J., Yao, X.-J., Weis, W. I., Stevens, R. C. & Kobilka, B. K. (2007). *Science*, **318**, 1266–1273.
Roth, M., Lewit-Bentley, A., Michel, H., Deisenhofer, J., Huber, R. & Oesterhelt, D. (1989). *Nature (London)*, **340**, 659–662.
Tao, M., Casutt, M. S., Fritz, G. & Steuber, J. (2008). *Biochim. Biophys. Acta*, **1777**, 696–702.
Tao, M., Türk, K., Diez, J., Grütter, M. G., Fritz, G. & Steuber, J. (2006). *Acta Cryst.* F**62**, 110–112.
Timmins, P. (1995). *Phys. B Condens. Matter*, **213**, 26–30.
Türk, K., Puhar, A., Neese, F., Bill, E., Fritz, G. & Steuber, J. (2004). *J. Biol. Chem.* **279**, 21349–21355.